Supporting Information for "Are Creep Events Big: Estimating Along Strike Lengths?"

Daniel B. Gittins[1], Jessica C. Hawthorne[1]

[1]Department of Earth Sciences, University of Oxford, Oxford, UK

Contents of this file

1. Supplementary Text S1
2. Figures S1 to S25

Additional Supporting Information (Files uploaded separately)

1. Creep catalog
2. Creep Booklet: Scaled to event
3. Creep Booklet: Scaled to all creepmeters

Introduction This supplementary information consists of four parts. In part 1, we provide a more detailed methodology of our creep event detections. Part 2 consists of CSV files containing our various creep event catalogs used in our multi-creepmeter event detections. Part 3 is the two creep booklets used in this study. Part 4 includes all

---

Corresponding author: D. B. Gittins, Department of Earth Sciences, University of Oxford, Oxford, UK. (daniel.gittins@earth.ox.ac.uk)

the supplementary figures referenced in the main text and figures of each creepmeter's percentages with every other creepmeter used in this study.

1. Supplementary Text S1

To study creep events in greater detail requires knowing when creep events occur in the creepmeter record. To detect creep events, we have used cross-correlation techniques to reduce the bias found in manual detections and produce more consistent start and end times. Before proceeding with the cross-correlation, we interpolated the creepmeter record to ensure that the data were spaced evenly at 10-minute intervals, except for Melendy Ranch (XMR) creepmeter, whose sampling frequency changed to 1-minute on 6^{th} September 2018. We, therefore, split the XMR record into two based on sampling frequency before proceeding.

Creep events at each creepmeter have different characteristic shapes; therefore, we picked a creep event for each creepmeter that captured the creepmeter's characteristic creep event shape that acted as a template for cross-correlation. We identified each template's start and end times before pre-processing to remove any error in the start time introduced during these processes. Then, the templates were extracted from the processed creep record using their start and end times before conducting the cross-correlation.

We removed a background trend from each creepmeter record so that creep events are easier to isolate within the creep record. In addition, we applied a zero-phase Butterworth bandpass filter at periods of 2 h and 5 days to remove short- and long-period noise in the creepmeter record. Filtering the creepmeter data improved detection accuracy as it reduces error in the start time of the creep event and removes long period non creep event-related trends.

Using our template timings, we conducted a rough cross-correlation for each creepmeter on the filtered creep event record. We identified peaks in the cross-correlation that exceeded a creepmeter dependant threshold between 0.05 and 0.2, allowing only one peak per 40 minutes. These thresholds were set relatively low, allowing for many false positives so that creep events that had a different shape could still be identified. These peak times were treated as potential creep events; however, their star times needed improvement. We estimated the start time of these potential events by examining the running average of the slip in hourly windows just before and after the cross-correlation peak. For the creepmeters north of Slacks Canyon (XSC), this time window varied from 1-5 days before the potential start time and 12 hours afterward. Creepmeters south of XSC required a shorter variable window of 6hrs to 3 days before and 12 hours after the potential start time. The change in the length of the time window from north to south accounted for the difference in creep styles between the northern and southern ends of the creeping section. The creep event start time is identified as the first time the slip rate exceeds the background slip rate within the examined window. This threshold value varies from creepmeter to creepmeter but is always the value of the 99th percentile of the average slip in hourly windows for the entire creepmeter record.

To improve the start-time further, we also used a method involving the shape of a bandpass filtered creep event. When a creep event is bandpass filtered, it develops a characteristic shape in which it has a large trough where the event begins. We used this to improve the detection start-time by shifting the start-time to the bottom of the nearest trough to our previous start time estimate.

Once we identified the start time, we used a similar approach to find the end of the creep event. To estimate the end time of our potential events, we examined the running average of the slip in overlapping daily windows following the start time. We estimated the end time to be the first time after the start time that the slip rate fell below a threshold value that represented the average slip per day at the background slip rate. This threshold was different for events affected by 28th September 2004 Parkfield earthquake. For those creepmeters unaffected by the afterslip following the earthquake, the threshold was set at the 90th percentile of the daily slip for all of the windows used. However, a lower 80th percentile was used for events affected by this earthquake. This 80th percentile overestimates the length of creep events in the first nine months after the 2004 Parkfield earthquake. To better isolate the end time of creep events in these first nine months, we extract the daily slip windows for these nine months and determine the end time of events in these nine months at the 90th percentile of the daily slip windows.

Once the start and end times were deduced, we calculated the slip that occurred during the creep event by differencing the measured values of the slip from the start and end of the creep event. To validate the approach used in calculating the slip values, we conducted a power spectral analysis. For this approach to be valid, the noise on the creepmeter is required to be a form of random-walk noise as opposed to white noise. At long periods the power spectrum for each has a slope of -1.98$\pm$0.005. The only exception to this is creepmeter X461 which has a slope closer to -1.87$\pm$0.005. We believe this creepmeter does not have the same power spectrum slope. Its location is more problematic than the other creepmeters (steeper slope, rainfall influenced, and soil relaxation towards a nearby pipeline) (Roeloffs, 2001)). At shorter periods (<1hr), the power spectra become

frequency independent and more characteristic of white noise. If the slope of the power spectra is equal to 2, then the noise is classified as random-walk noise and is caused by small random motions of the geodetic instrument (Langbein et al., 1993; Langbein & Johnson, 1997). We have concluded that the majority of noise seen in the creepmeter data is in the form of random-walk noise. This validated the approach of taking slip measurements as the difference between a start and end-points as the error in the data between these two points is incorporated in the error of the slip measurement.

The initial set of detection includes very short duration detections that are steps between data points. These steps are caused by earthquakes, or stick-slip instrumental artifacts (Bilham & Castillo, 2020). We remove these steps by including the criteria that our creep event detections must be longer than 10 minutes in duration.

To make the detections more robust, we also removed some detections based on their slip. We find detections with tiny slip values are often found at times where the data is particularly noisy. To remove these, we isolated the top 10% largest slip values from each creepmeter's detections and identified a minimum slip threshold for the detection to be classified as a creep event. This threshold is set at 1% of the slip of the median value of the largest 10% of creep event detections at each creepmeter.

Creep events may have one or more steps within them, leading to double detections via the detection algorithm. The detection process distinguishes between multiple humped creep events and temporally close single hump creep events by determining if the daily slip value at the end of the first hump is small enough to fall below the creep event end threshold value. If the creep event has multiple humps, it will have two detections within the creep record (one for each hump), which will have the same end time. Therefore, we

remove duplicate events based on their end times as well as their start times. Following on from this, we have flagged any detections that have a start or end time that lies within the creep record that was filled in by interpolation. These detections are unreliable as their large slip values may be due to either the temporally short steps mentioned above or due to a creep event.

Once the detections have been through this process, they are plotted and checked manually to ensure only real creep events are carried forward into further work based on these creep events. These detections we remove usually consist of steps in the data surrounded by noise, meaning their start times are detected early, which increases their duration above the 10-minute duration cut-off designed to remove them.

A final manual correction was then completed on each real creep event detection to achieve the best possible pick for the start of the creep event guided by the start-time detected using the above approach. As a result, we have produced a finalized creep event catalog for each creepmeter, which included 2120 creep events.

2. Creep Catalog

Here, we provide a brief description of our creep event catalog. The 18 creepmeters used in this study have a creep event catalog, provided here as 18 CSV files. These catalogs include information on the start time of the creep event and its corresponding displacement. We have also included estimates of the end time, end displacement, and the slip and duration of the creep event. It is important to note that the end of a creep event is less well defined than the beginning; therefore, these end times are only to be used as a guide. The reader should determine the end of the creep event themselves if using these catalogs for future work.

Our catalog of multi-creepmeter events is also proved as a CSV file. This catalog is split into creepmeter columns. If an event is within 24hrs of another event at another creepmeter, then the start time of that event is included in the creepmeter column, with potential multi-creepmeter events lying on the same row. Thus, this catalog does include all events within 24hrs of one another. It, therefore, should be interpreted and used after consultation of the relevant Figures S1-S17, which provide the percentage of creep events observed at each creepmeter pair, indicating if the relationship between these events is genuine or likely have occurred by chance.

Data Set S1. Catalog of creep events recorded at the San Juan Bautista (XSJ2/XSJ3) creepmeter as a csv file.

Data Set S2. Catalog of creep events recorded at the Harris Ranch (XHR2/XHR3) creepmeter as a csv file.

Data Set S3. Catalog of creep events recorded at the Cienega Winery Central (CWC3) creepmeter as a csv file.

Data Set S4. Catalog of creep events recorded at the Cienega Winery North (CWN1) creepmeter as a csv file.

Data Set S5. Catalog of creep events recorded at the Melendy Ranch (XMR1) creepmeter as a csv file.

Data Set S6. Catalog of creep events recorded at the Slacks Canyon (XSC1) creepmeter as a csv file.

Data Set S7. Catalog of creep events recorded at the Middle Mountain (XMM1) creepmeter as a csv file.

Data Set S8. Catalog of creep events recorded at the Middle Ridge (XMD1) creepmeter as a csv file.

Data Set S9. Catalog of creep events recorded at the Varian (XVA1) creepmeter as a csv file.

Data Set S10. Catalog of creep events recorded at the Roberson, SW trace (XRSW) creepmeter as a csv file.

Data Set S11. Catalog of creep events recorded at the Parkfield (XPK1/XPK2) creepmeter as a csv file.

Data Set S12. Catalog of creep events recorded at the Taylor Ranch (XTA1) creepmeter as a csv file.

Data Set S13. Catalog of creep events recorded at the Hearst, SW trace (XHSW) creepmeter as a csv file.

Data Set S14. Catalog of creep events recorded at the Work Ranch (WKR1) creepmeter as a csv file.

Data Set S15. Catalog of creep events recorded at the Carr Ranch (CRR1) creepmeter as a csv file.

Data Set S16. Catalog of creep events recorded at the Gold Hill (XGH1) creepmeter as a csv file.

Data Set S17. Catalog of creep events recorded at the Highway 46 (C46) creepmeter as a csv file.

Data Set S18. Catalog of creep events recorded at the Highway 46 (X46) creepmeter as a csv file.

Data Set S19. Catalog of creep events recorded within 24 hours of a creep event at another creepmeter as a csv file.

3. Creep Booklets

Here we include two booklets depicting creep events; one scaled to the creep event itself and another scaled to the maximum slip of all of the records. Each page of the booklet includes one creep event, with the time of the event and the creepmeter that recorded it noted at the top of the page. We have stacked the creepmeter records one on top of another, with the most northern creepmeter (XSJ) at the top and the most southern creepmeter (X46) at the bottom. The start and end times of the creep event are shown as vertical dashed lines across all plots, and the event is shown in color. If another event at another creepmeter occurs in the window plotted, we highlight this by giving that trace a faint color with vertical dashed grey lines to highlight the event on that plot only. All of the plots are rescaled so that the creep event's start time is when all of the creepmeter traces will cross the x-axis.

Data Set S20. Booklet of creep events scaled to the event itself.

Data Set S21. Booklet of creep events scaled to the maximum slip in the window of all of the 18 creepmeters.

References

Bilham, R., & Castillo, B. (2020). The July 2019 Ridgecrest, California, Earthquake Sequence Recorded by Creepmeters: Negligible Epicentral Afterslip and Prolonged Triggered Slip at Teleseismic Distances. *Seismological Research Letters*, *91*(2A), 707–720. doi: 10.1785/0220190293

Langbein, J., & Johnson, H. (1997). Correlated errors in geodetic time series: Implications for time-dependent deformation. *Journal of Geophysical Research: Solid Earth*, *102*(B1), 591–603. Retrieved from `https://agupubs.onlinelibrary.wiley.com/doi/abs/10.1029/96JB02945` doi: https://doi.org/10.1029/96JB02945

Langbein, J., Quilty, E., & Breckenridge, K. (1993). Sensitivity of crustal deformation instruments to changes in secular rate. *Geophys. Res. Lett.*, *20*(2), 85–88. doi: 10.1029/92GL02718

Roeloffs, E. A. (2001). Creep rate changes at Parkfield, California 1966-1999: Seasonal, precipitation induced, and tectonic. *J. Geophys. Res.*, *106*(B8), 16525–16547. doi: 10.1029/2001JB000352

do not specify file extension

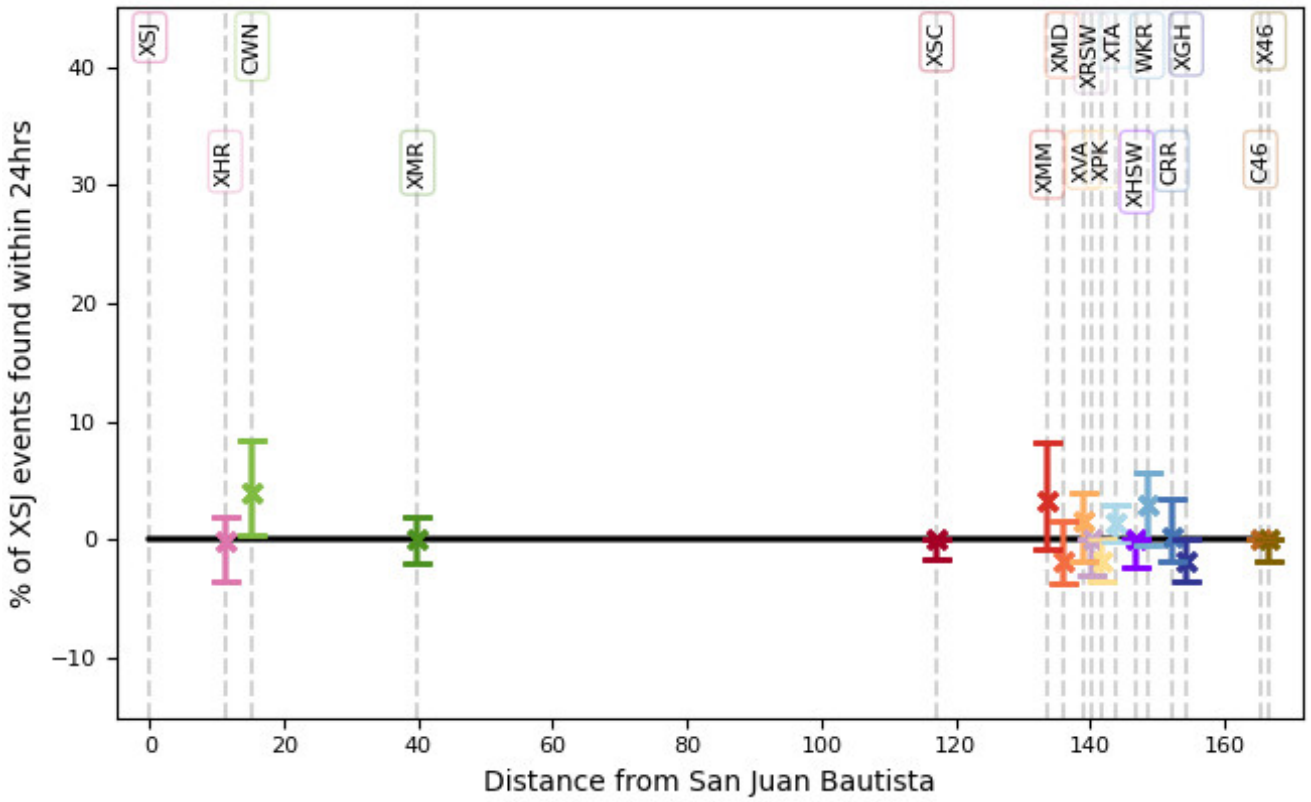

Figure S1. Percentage of XSJ events observed at all other creepmeters, scaled with distance.

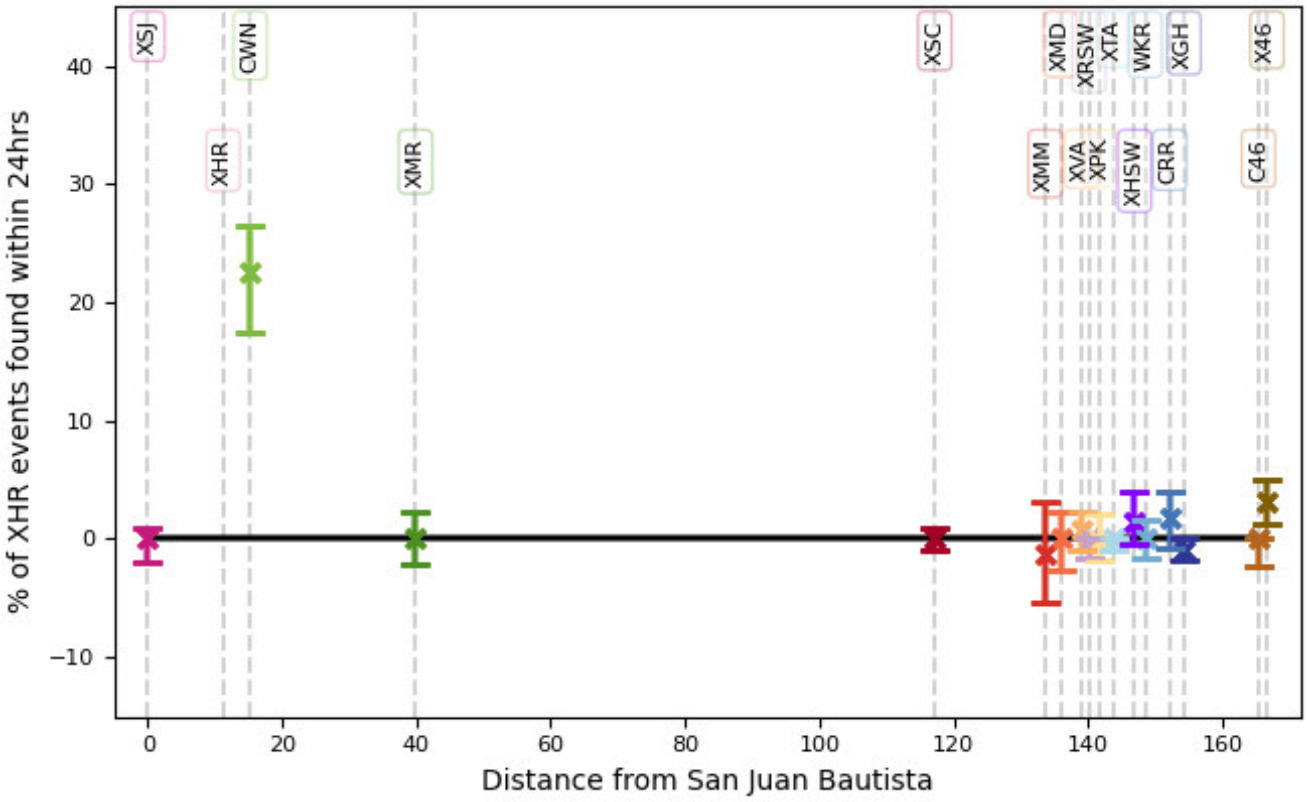

Figure S2. Percentage of XHR events observed at all other creepmeters, scaled with distance.caption

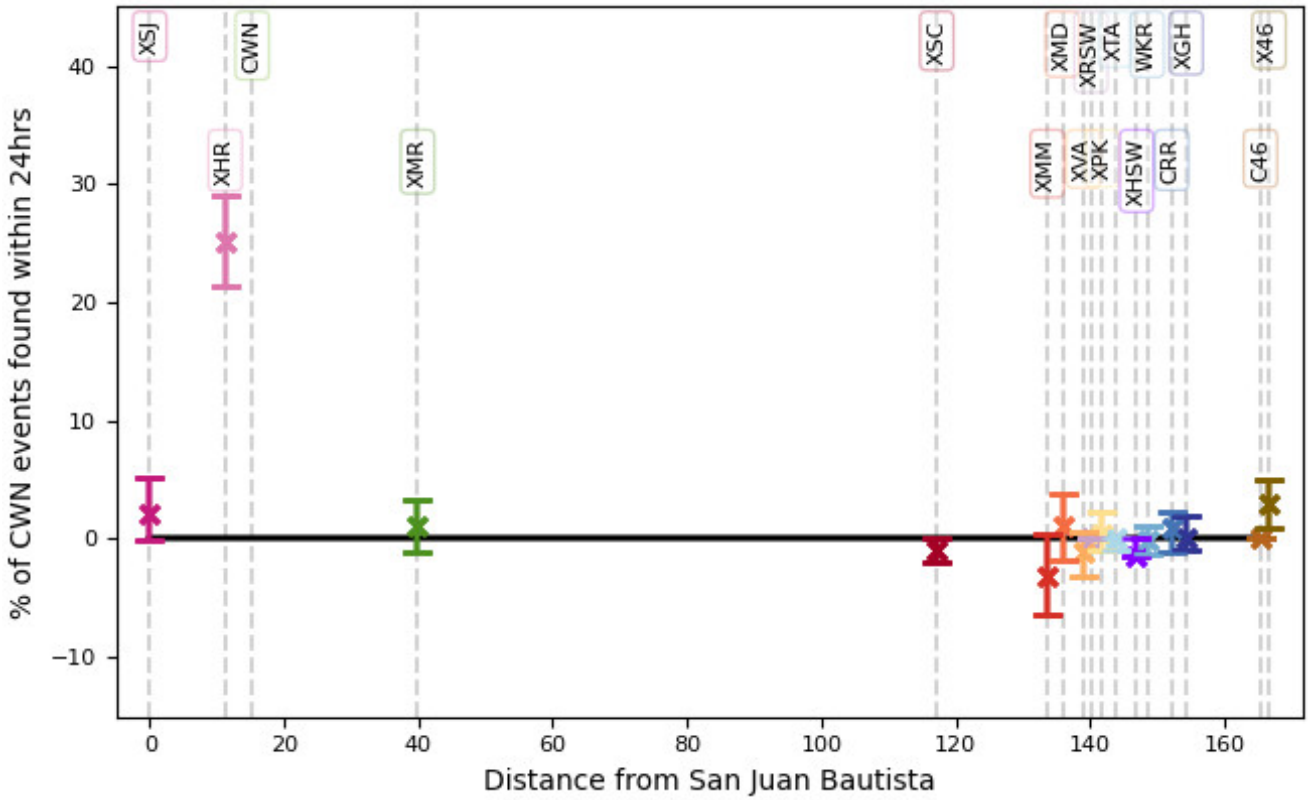

Figure S3. Percentage of CWN events observed at all other creepmeters, scaled with distance.caption

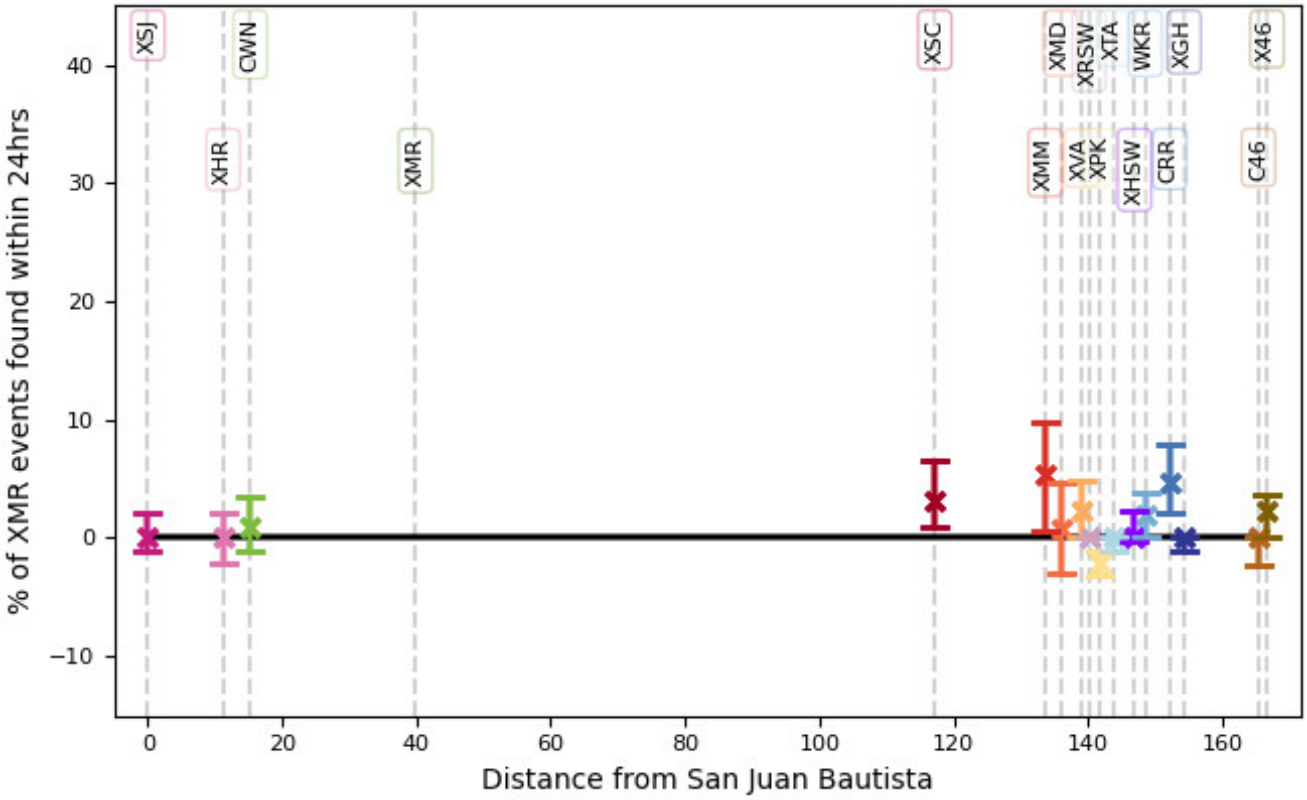

Figure S4. Percentage of XMR events observed at all other creepmeters, scaled with distance.

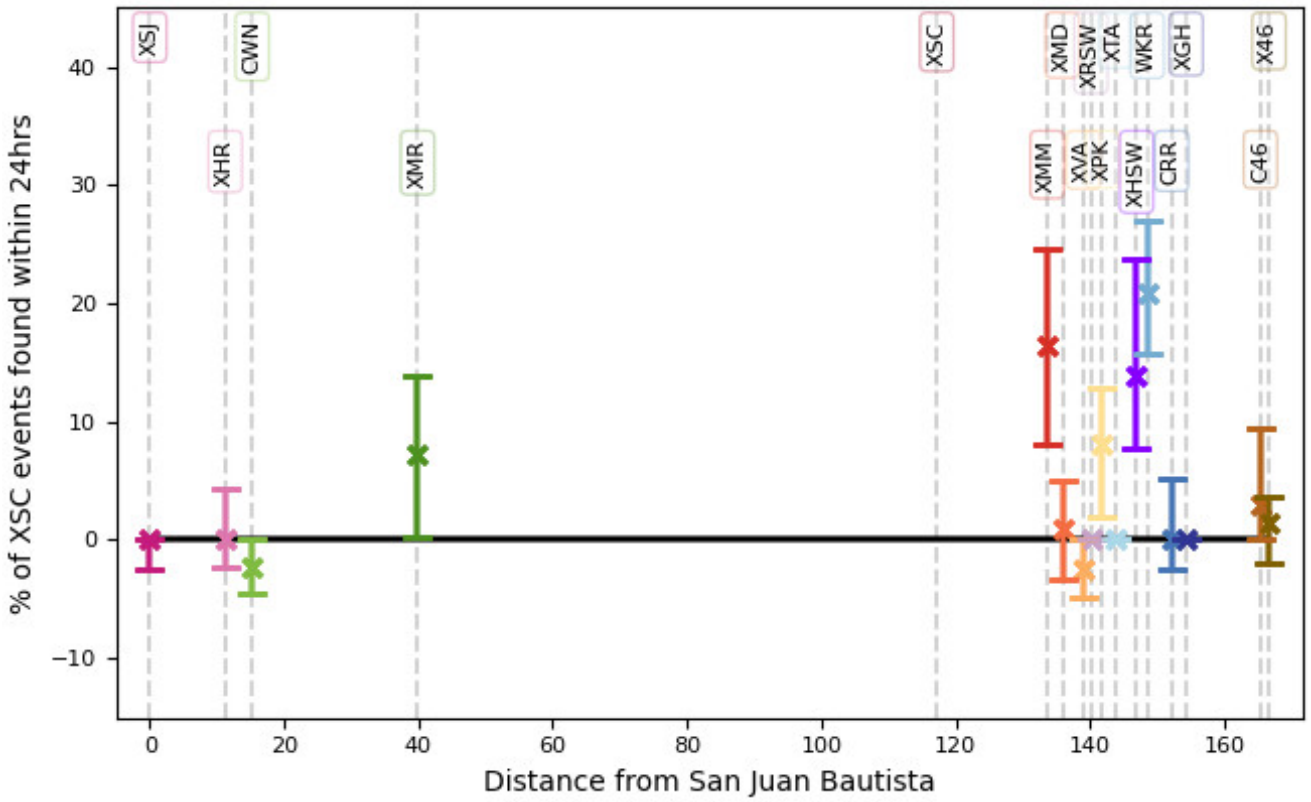

Figure S5. Percentage of XSC events observed at all other creepmeters, scaled with distance.

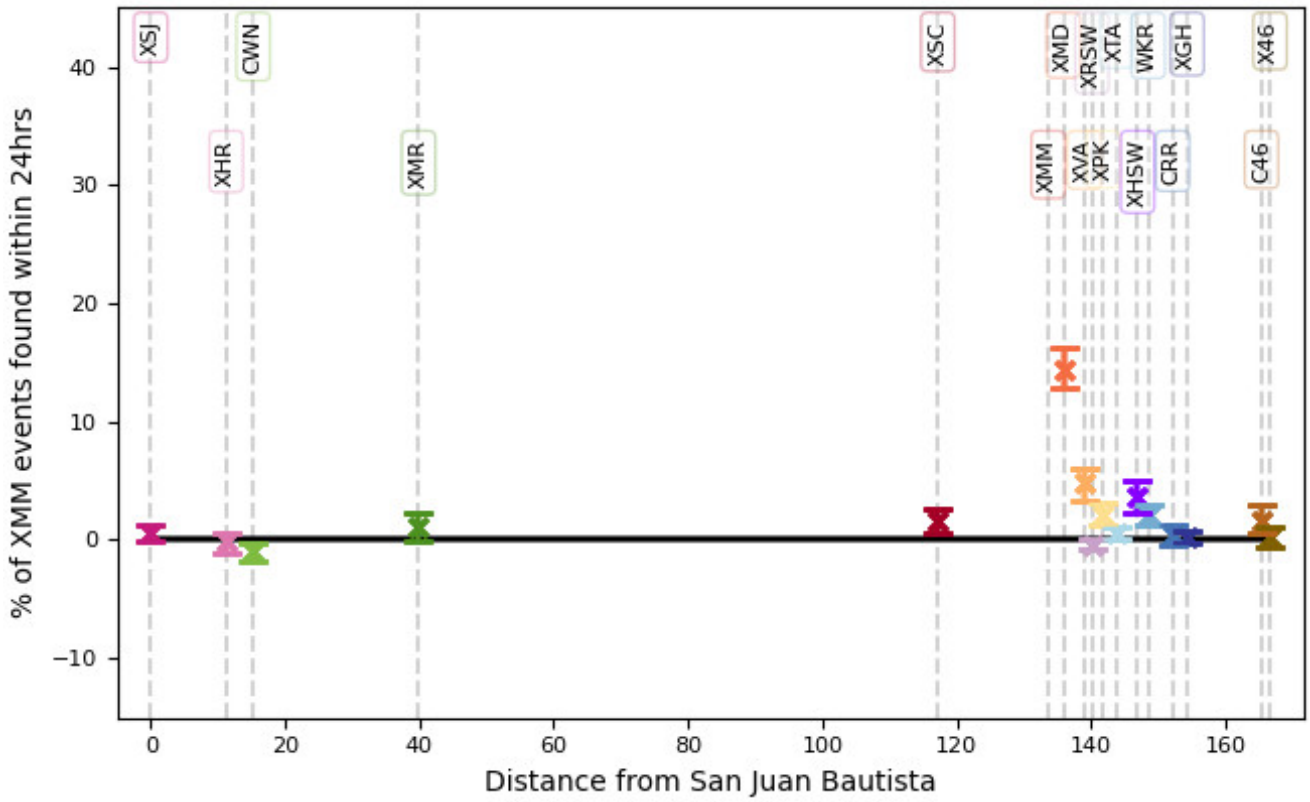

Figure S6. Percentage of XMM events observed at all other creepmeters, scaled with distance.

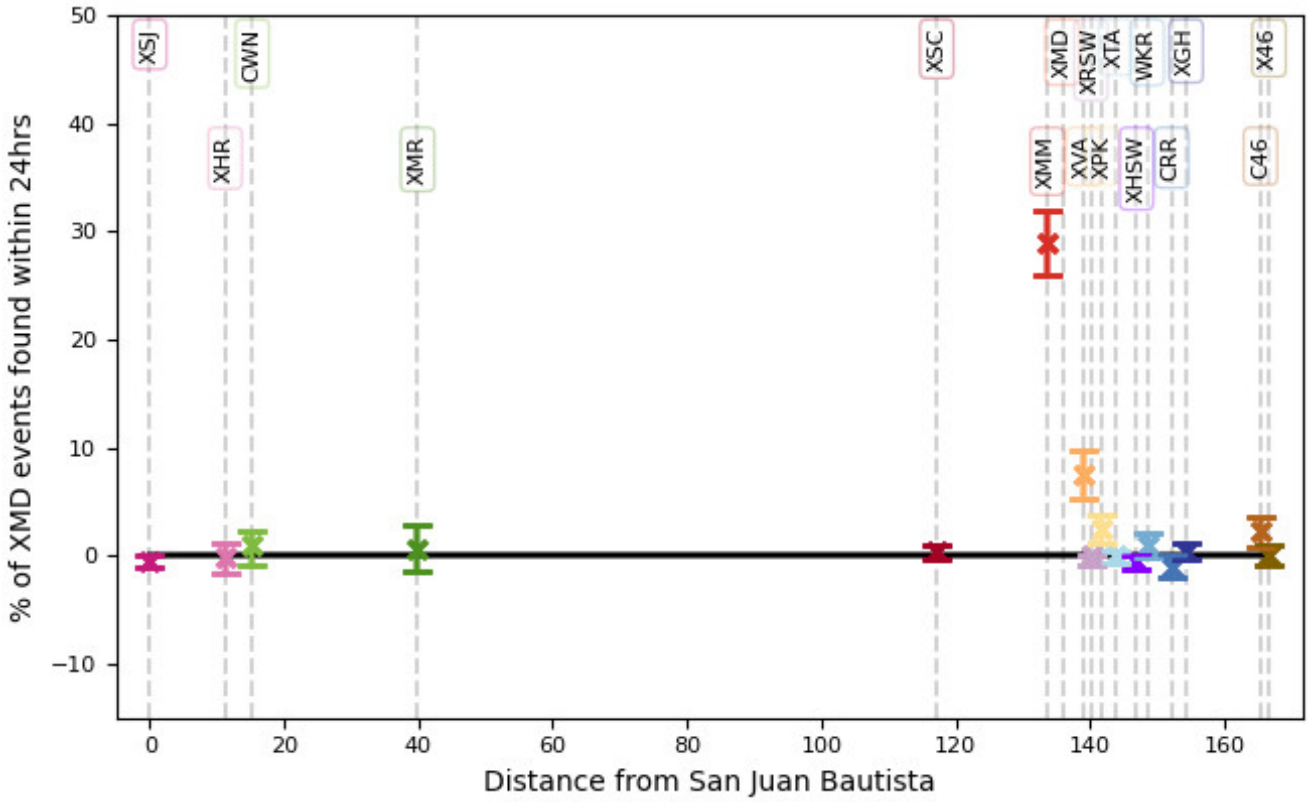

Figure S7. Percentage of XMD events observed at all other creepmeters, scaled with distance.

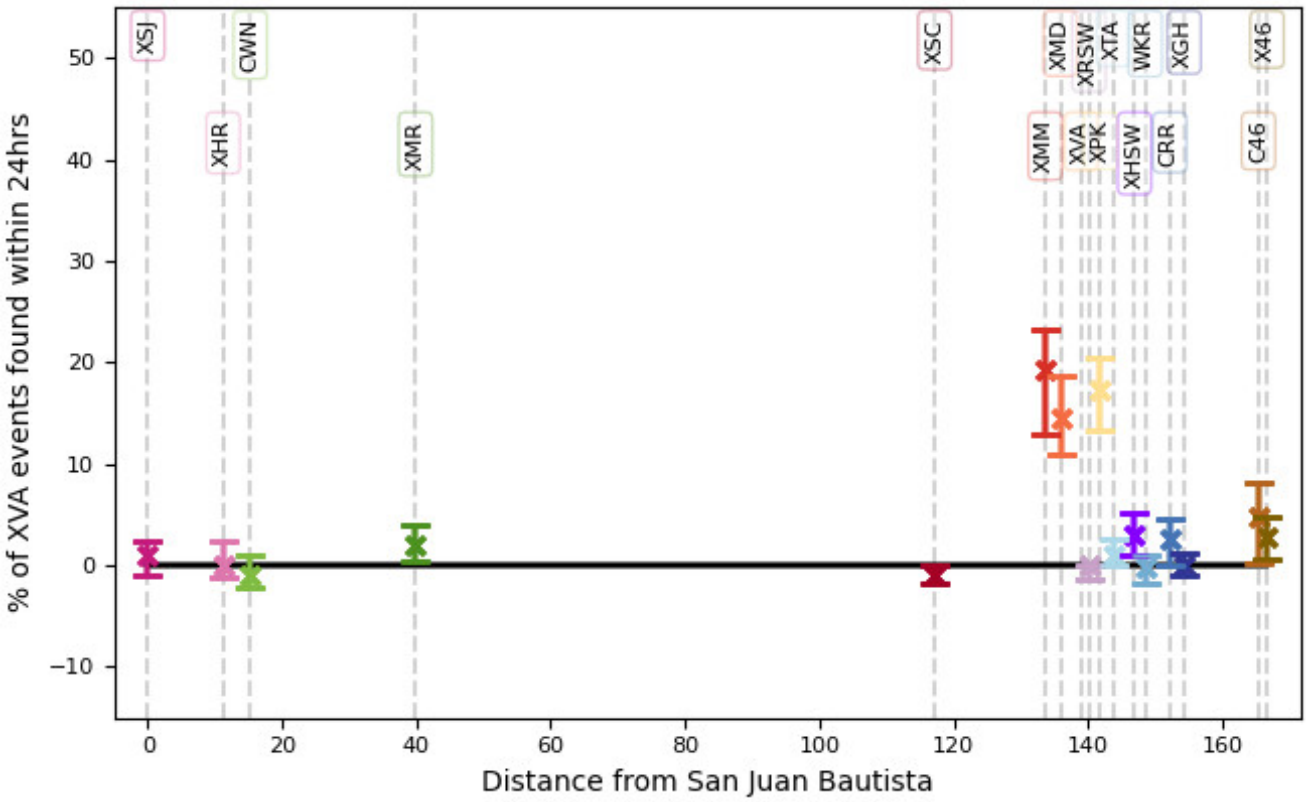

Figure S8. Percentage of XVA events observed at all other creepmeters, scaled with distance.

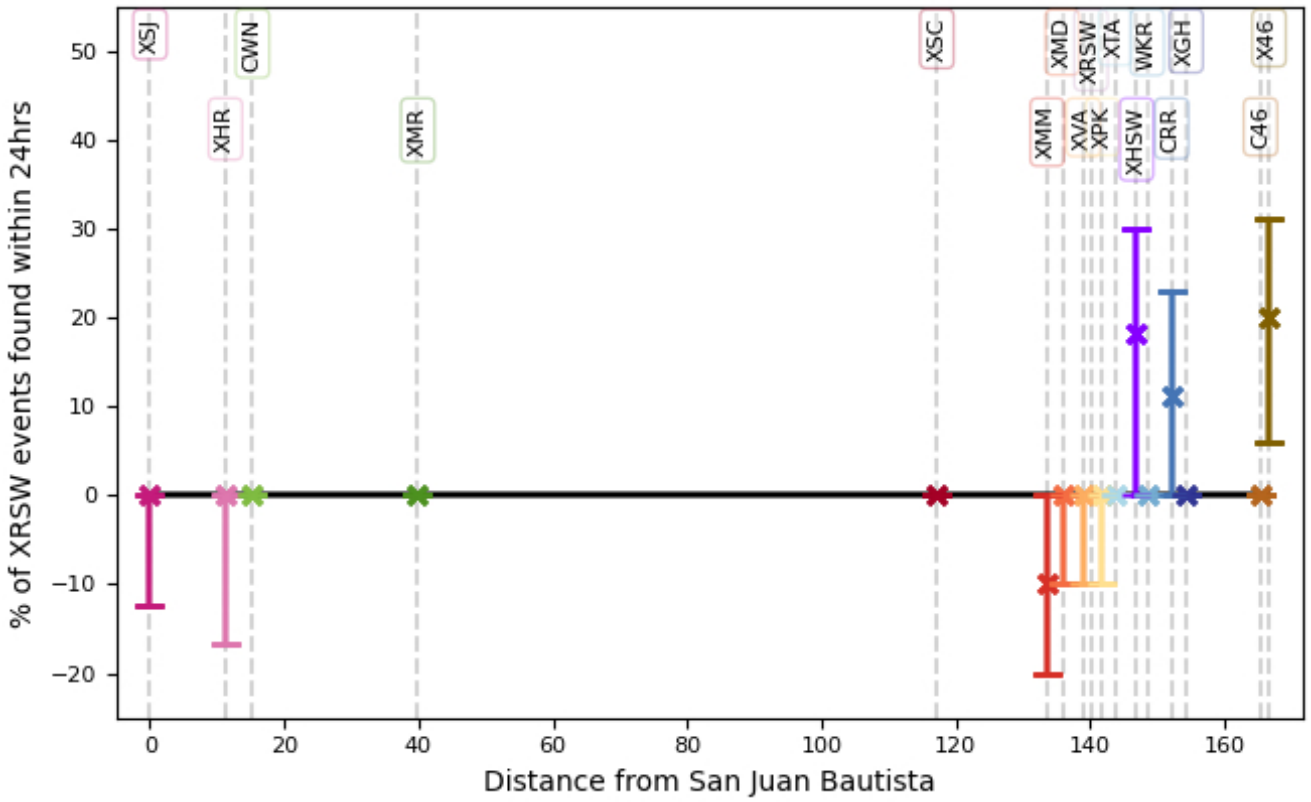

Figure S9. Percentage of XRSW events observed at all other creepmeters, scaled with distance.

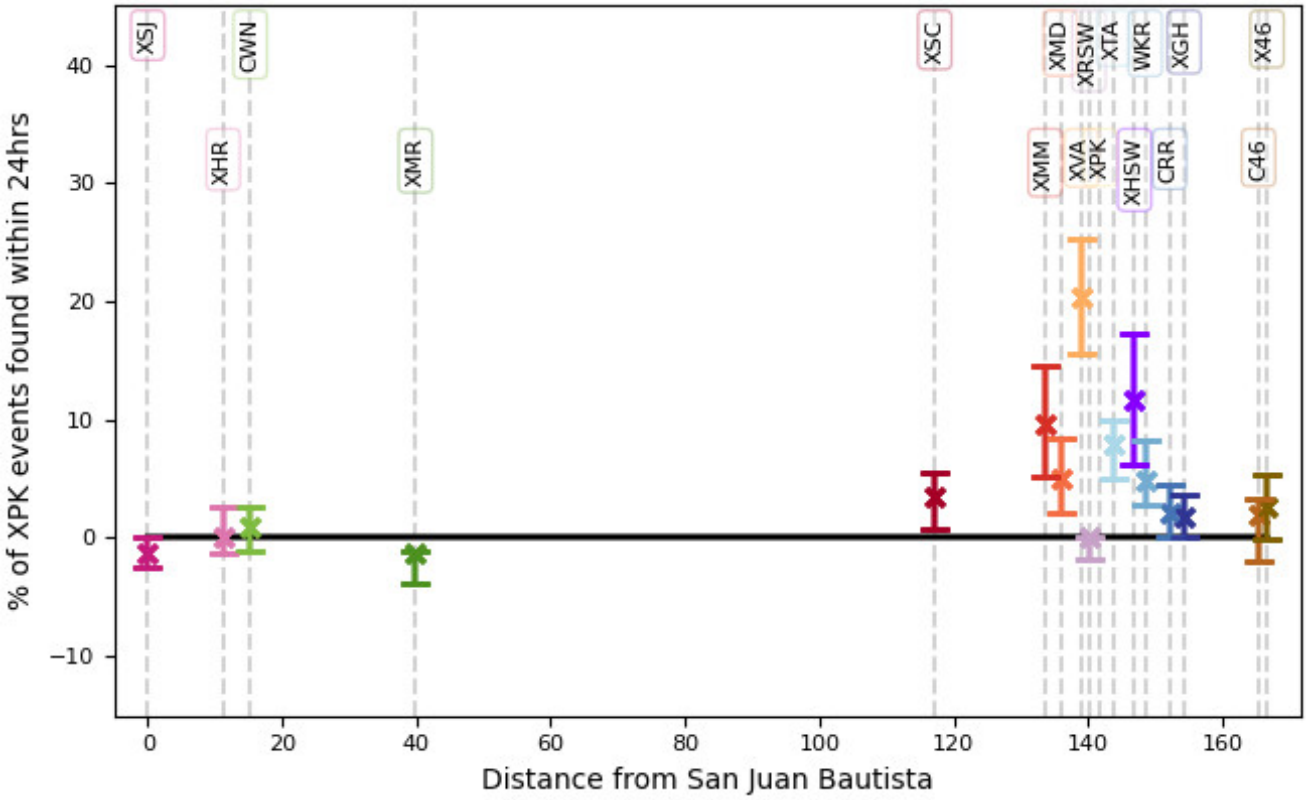

Figure S10. Percentage of XPK events observed at all other creepmeters, scaled with distance.

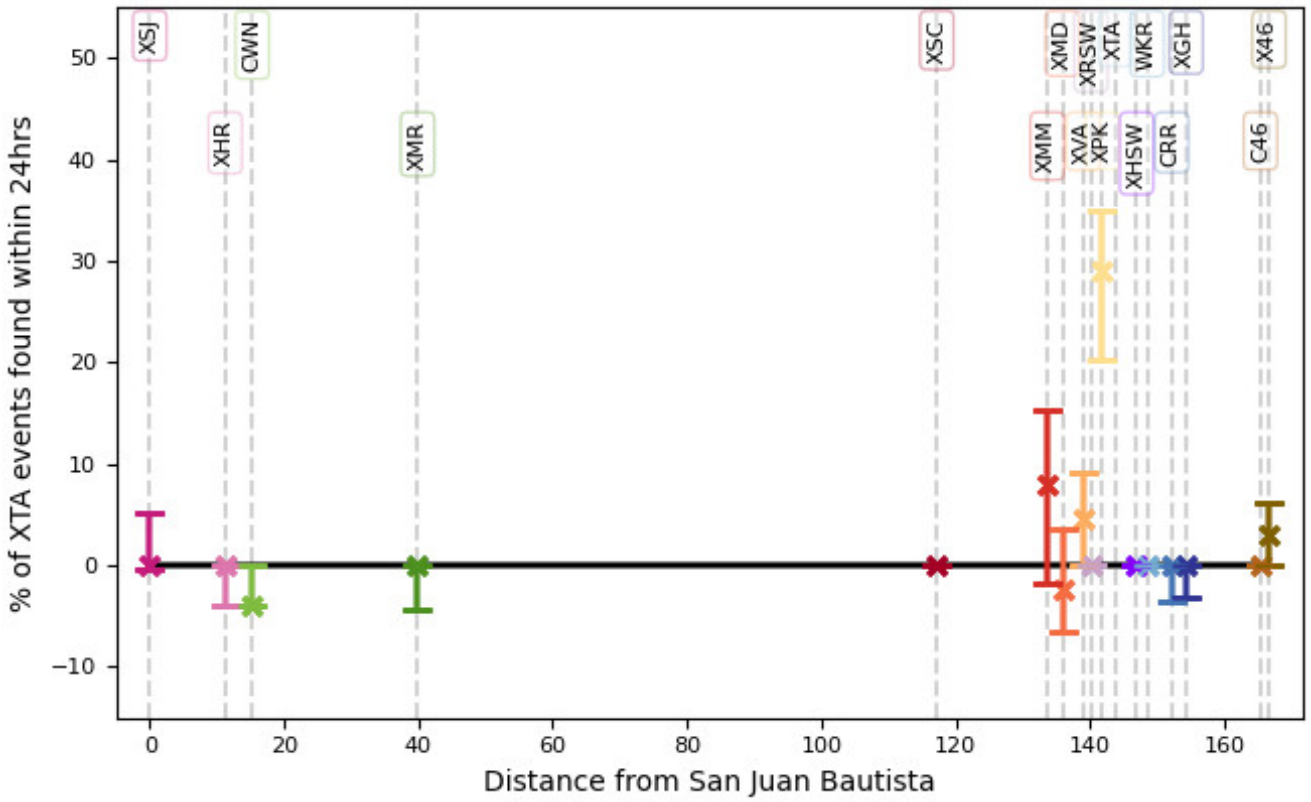

Figure S11. Percentage of XTA events observed at all other creepmeters, scaled with distance.

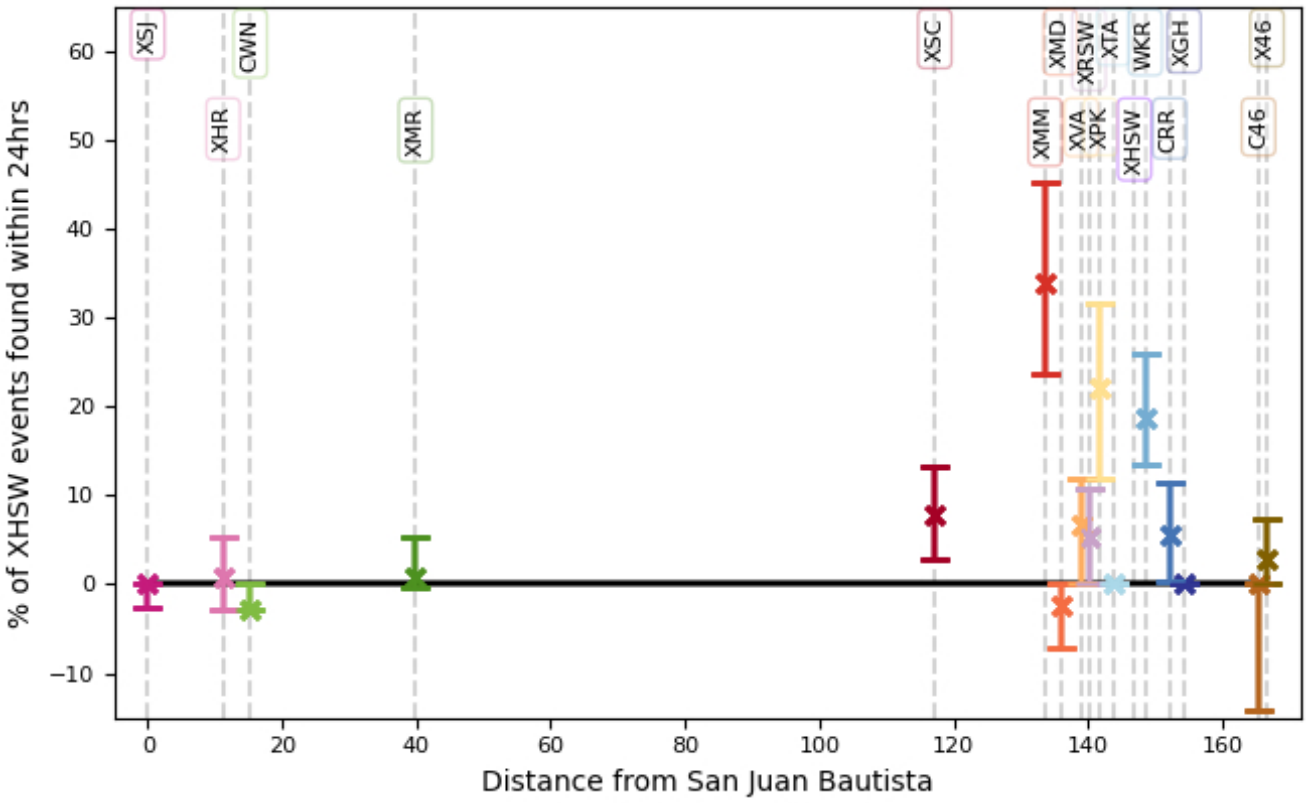

Figure S12. Percentage of XHSW events observed at all other creepmeters, scaled with distance.

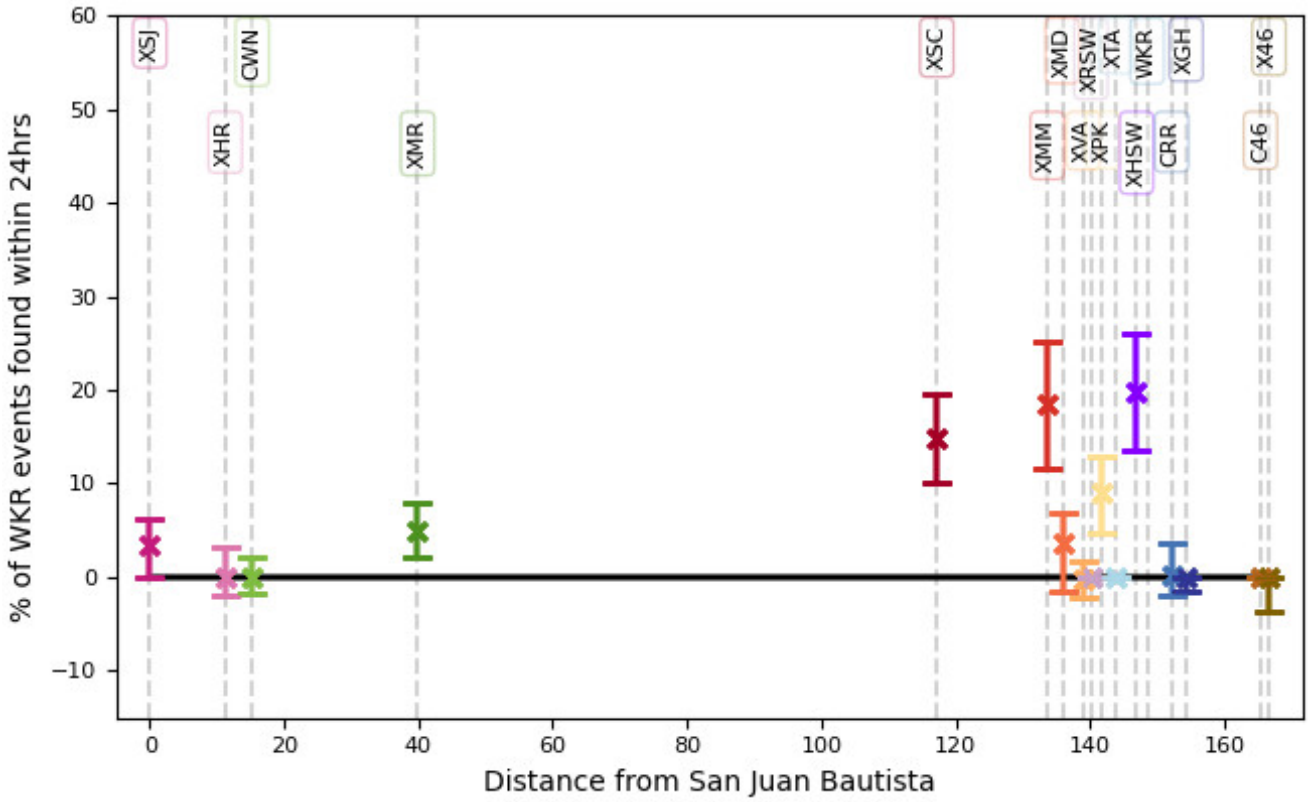

Figure S13. Percentage of WKR events observed at all other creepmeters, scaled with distance.

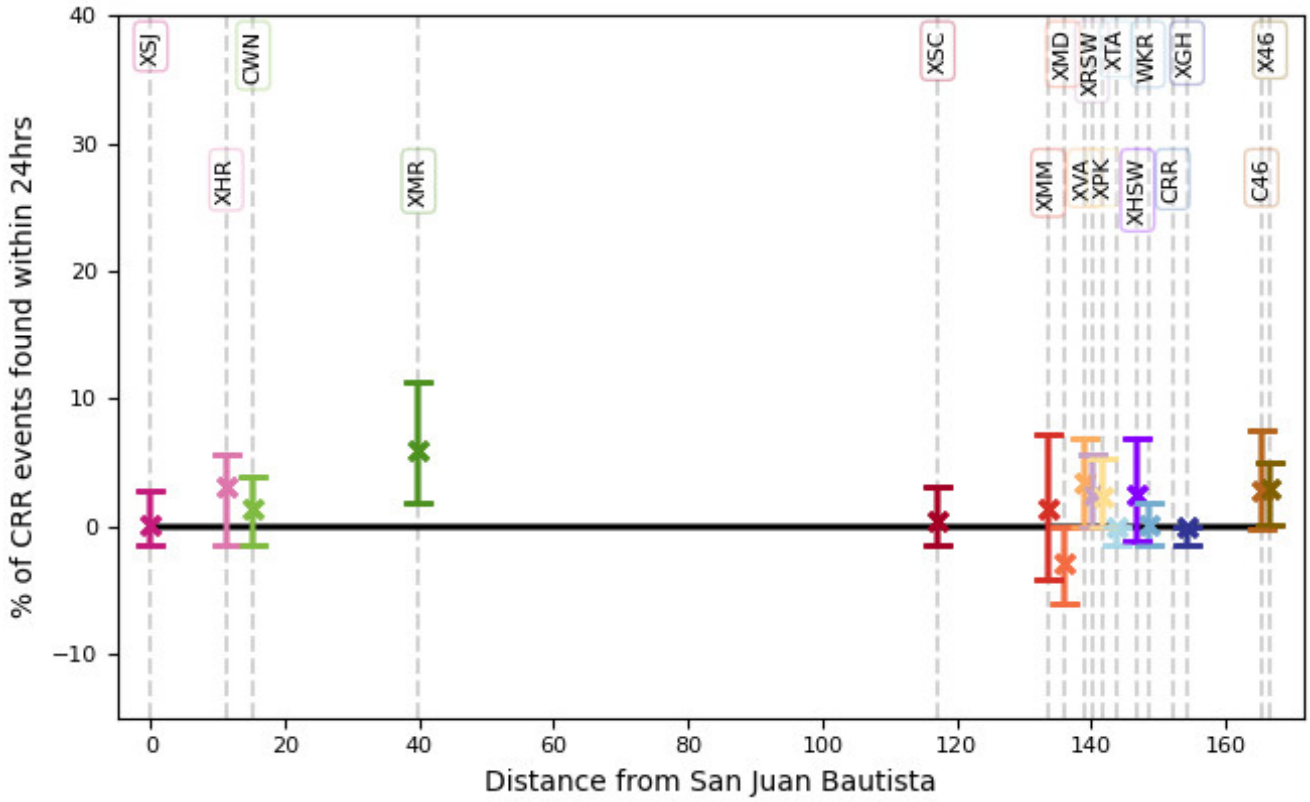

Figure S14. Percentage of CRR events observed at all other creepmeters, scaled with distance.

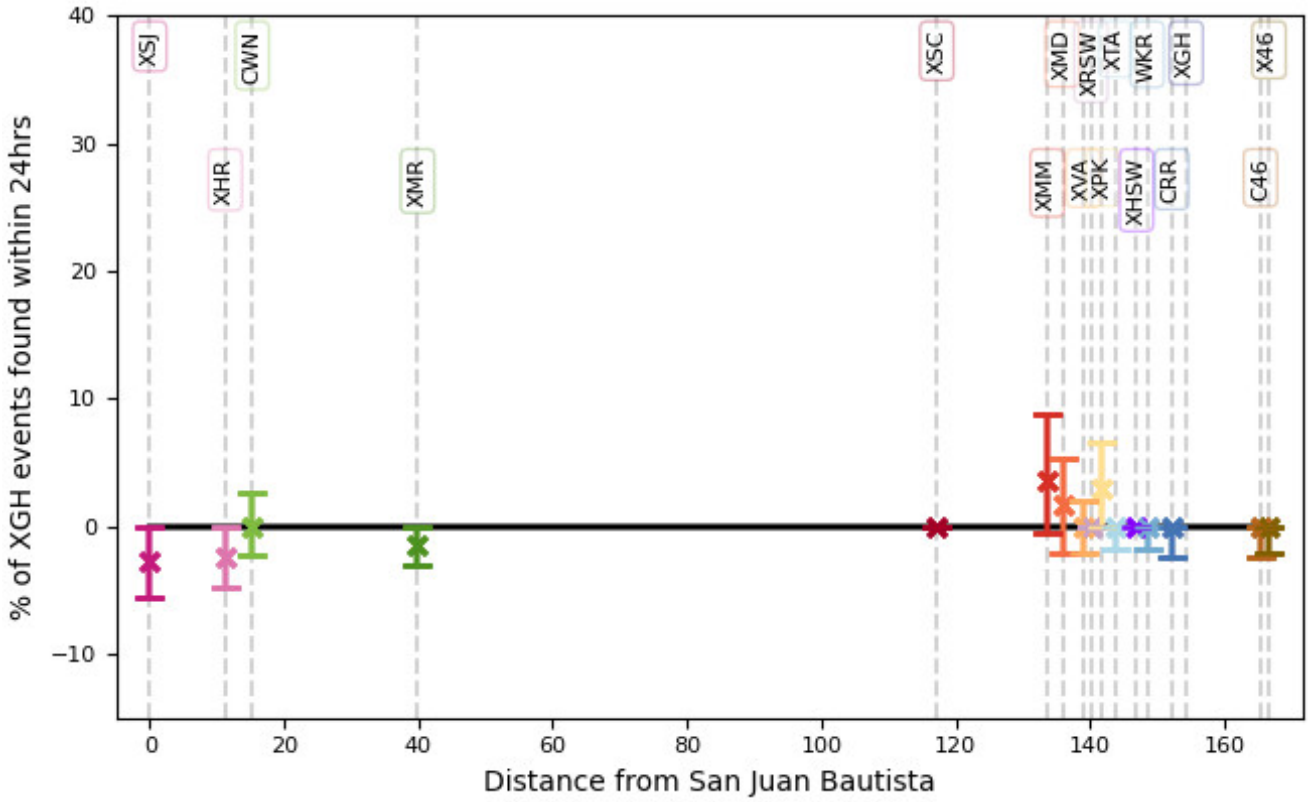

Figure S15. Percentage of XGH events observed at all other creepmeters, scaled with distance.

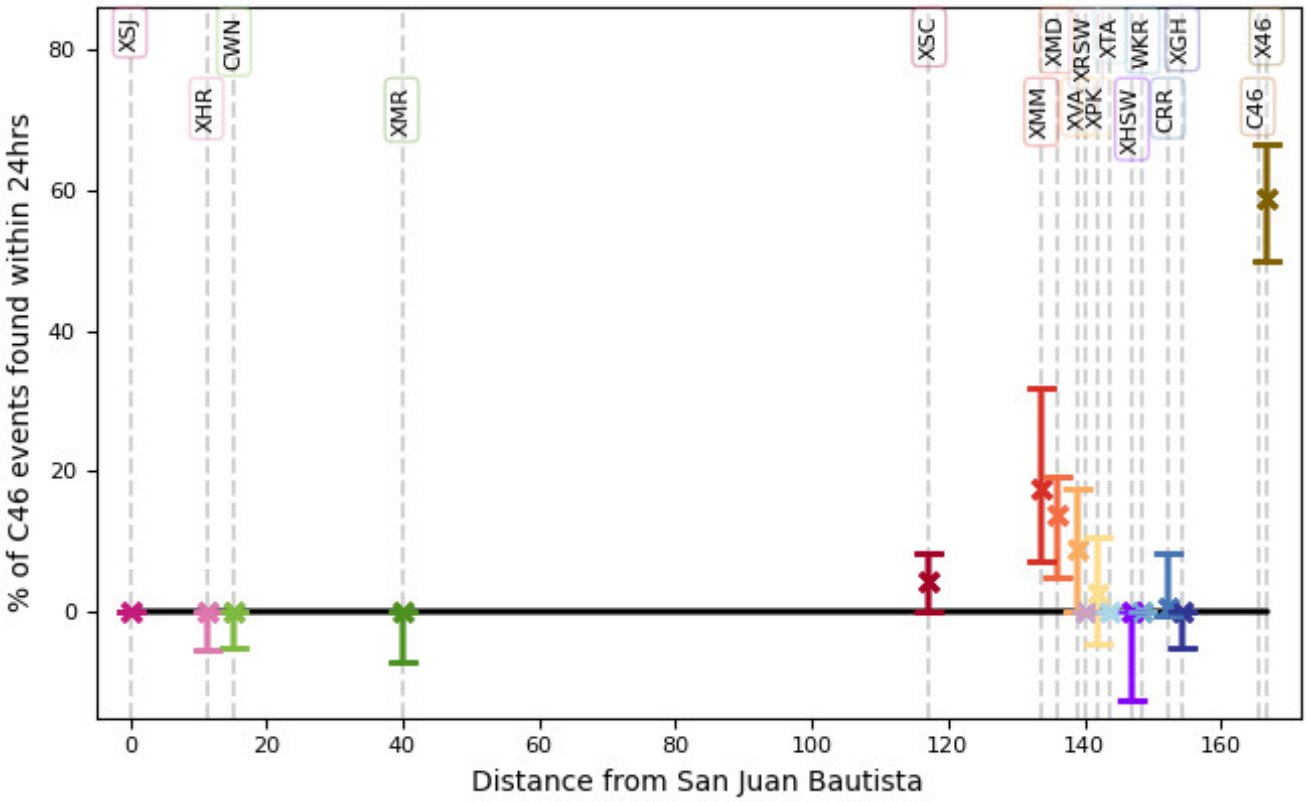

Figure S16. Percentage of C46 events observed at all other creepmeters, scaled with distance.

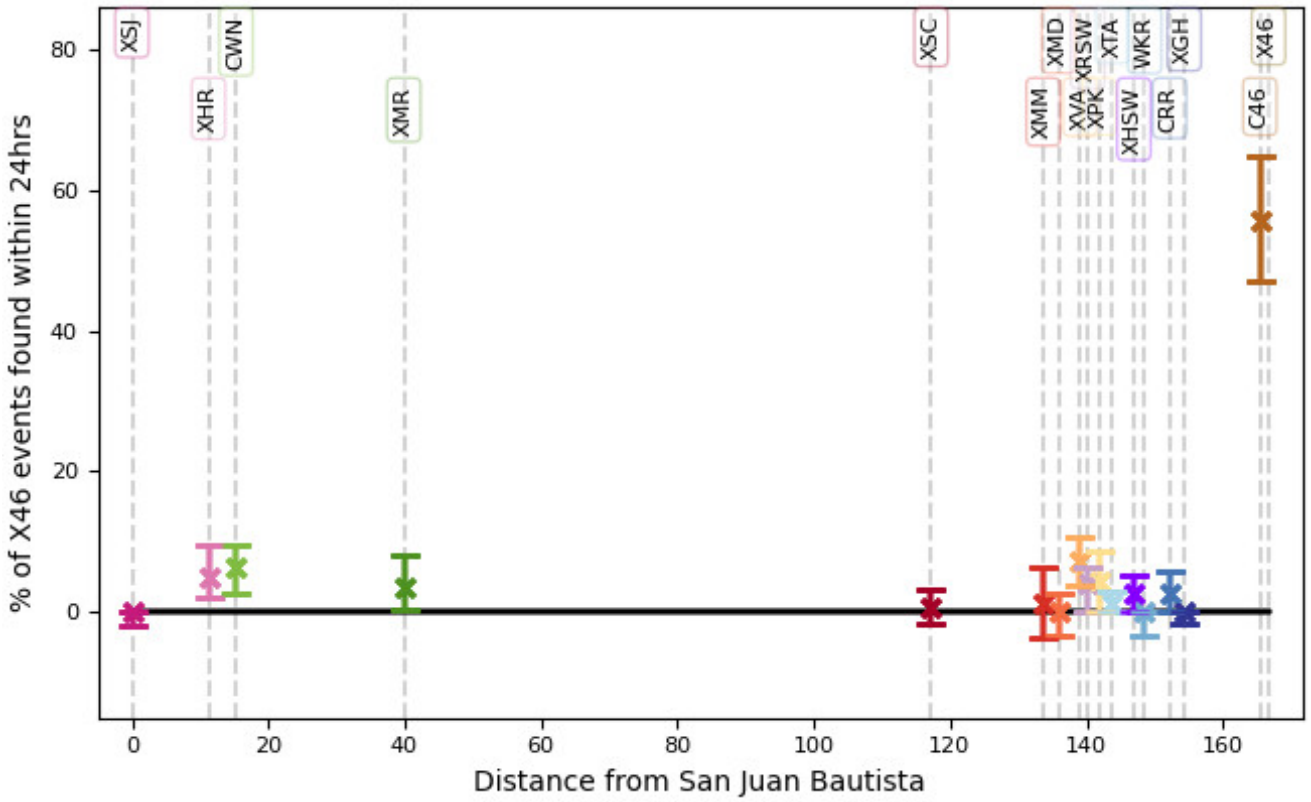

Figure S17. Percentage of X46 events observed at all other creepmeters, scaled with distance.

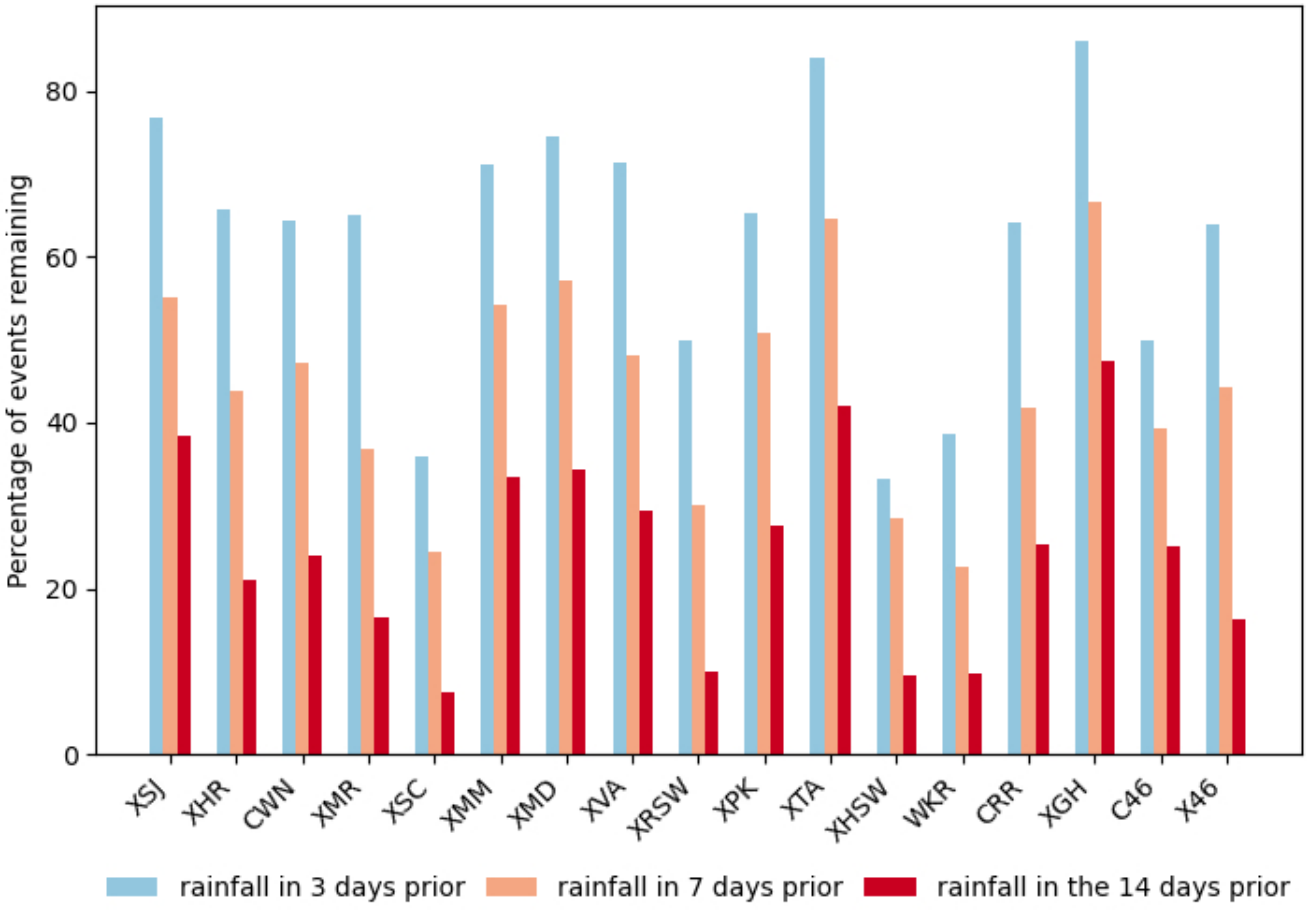

Figure S18. Percentage of creep events remaining when events with rainfall in the 3- (light blue), 7- (orange), and 14-days (red) before the event are removed.

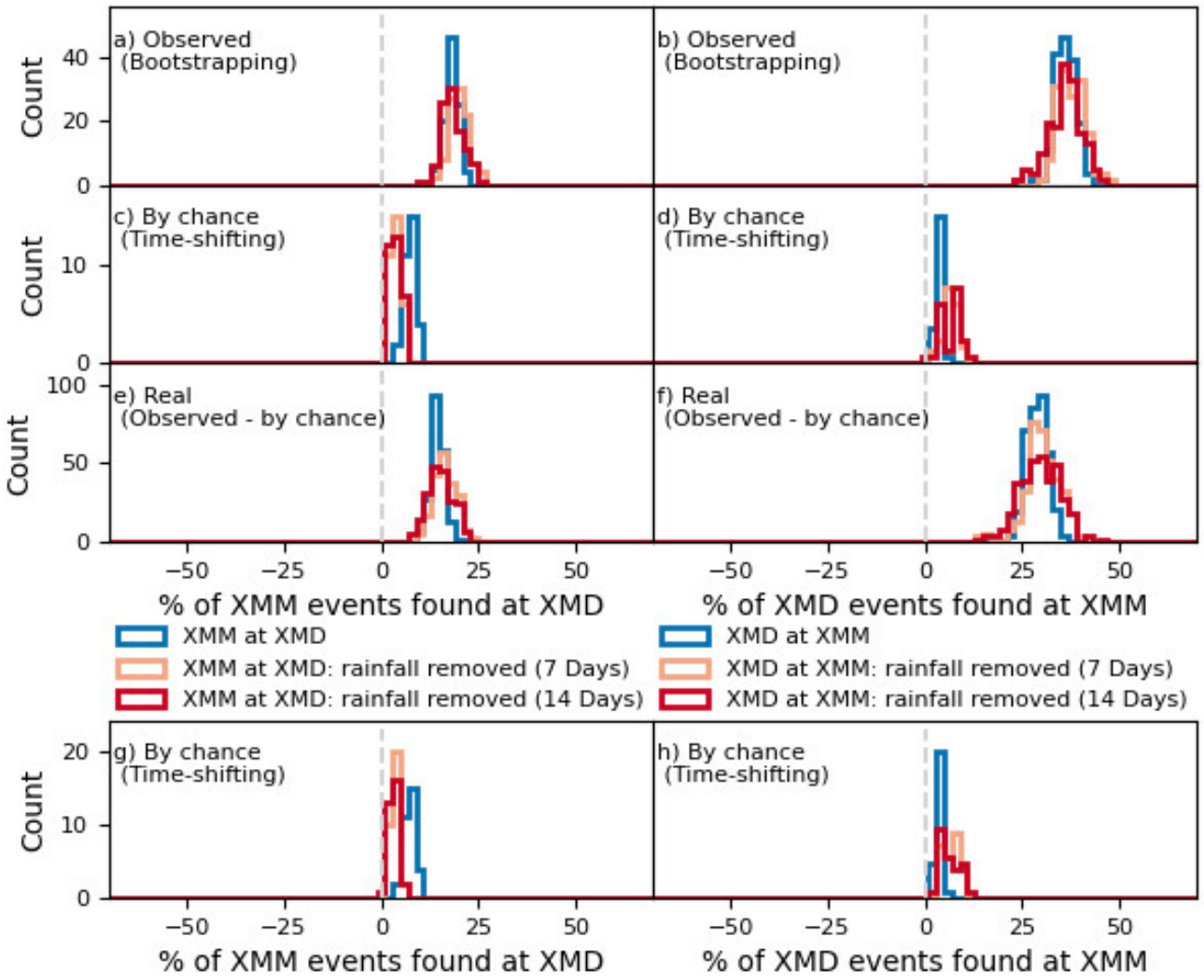

Figure S19. Rainfall analysis histograms for Middle Mountain (XMM) and Middle Ridge (XMD). Blue historgrams are the original analysis before rainfall was removed, orange and red histograms are for when events with rainfall in the 7 or 14 days prior are removed respectively. a) and b) are the bootstrapped distributions of the percentage of events with different amounts of rainfall accounted for. c) and d) shows the percentage of time correlated events that are occuring by chance. e) and f) are percentage of events that are detected at both creepmetes when by chance occurances are removed. g) and h) show the percentage of events that are observed at one creepmeter given seasonality and rain at the other

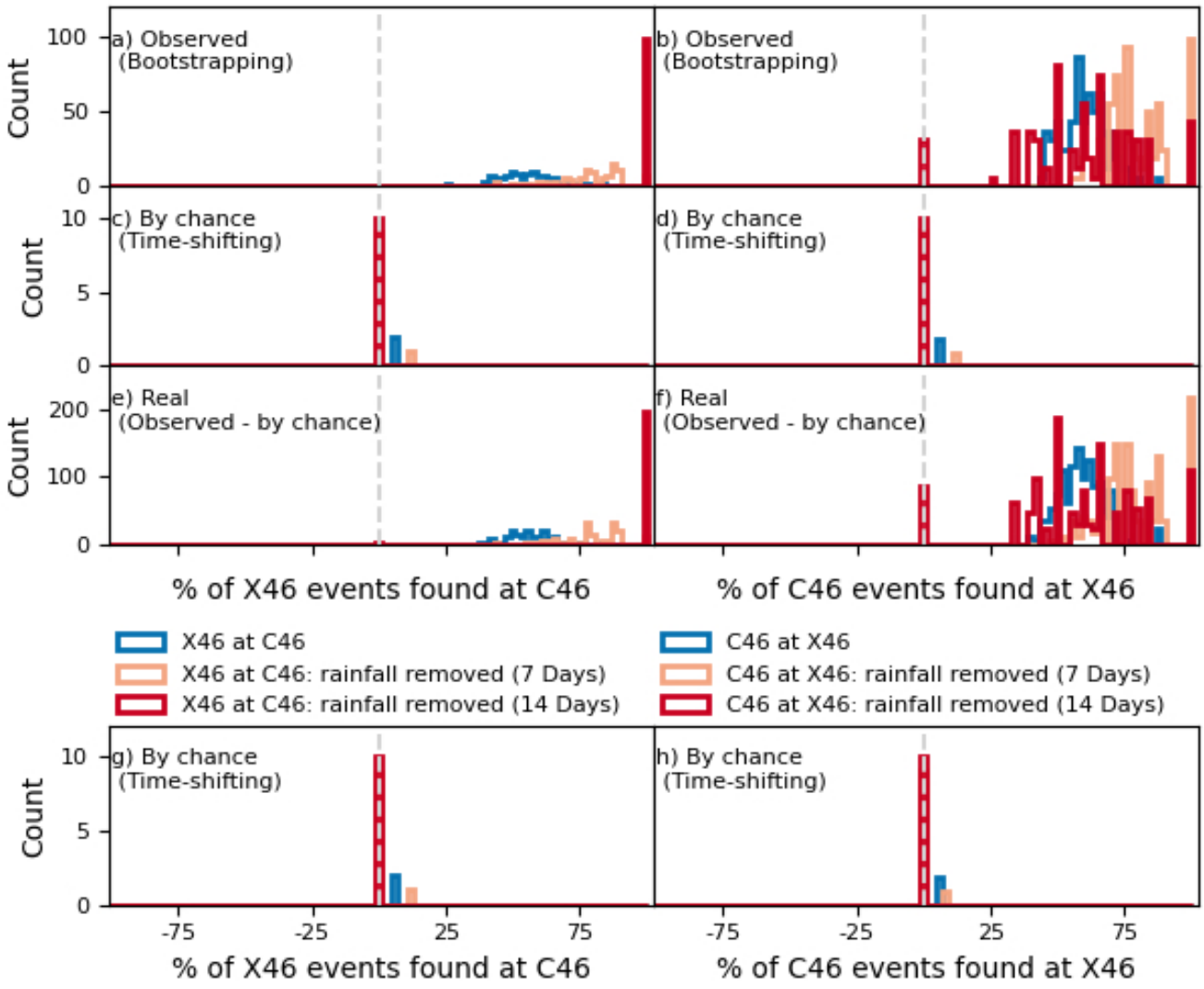

Figure S20. Rainfall analysis histograms for Highway 46 (X46/C46). Blue historgrams are the original analysis before rainfall was removed, orange and red histograms are for when events with rainfall in the 7 or 14 days prior are removed respectively. a) and b) are the bootstrapped distributions of the percentage of events with different amounts of rainfall accounted for. c) and d) shows the percentage of time correlated events that are occuring by chance. e) and f) are percentage of events that are detected at both creepmetes when by chance occurances are removed. g) and h) show the percentage of events that are observed at one creepmeter given seasonality and rain at the other

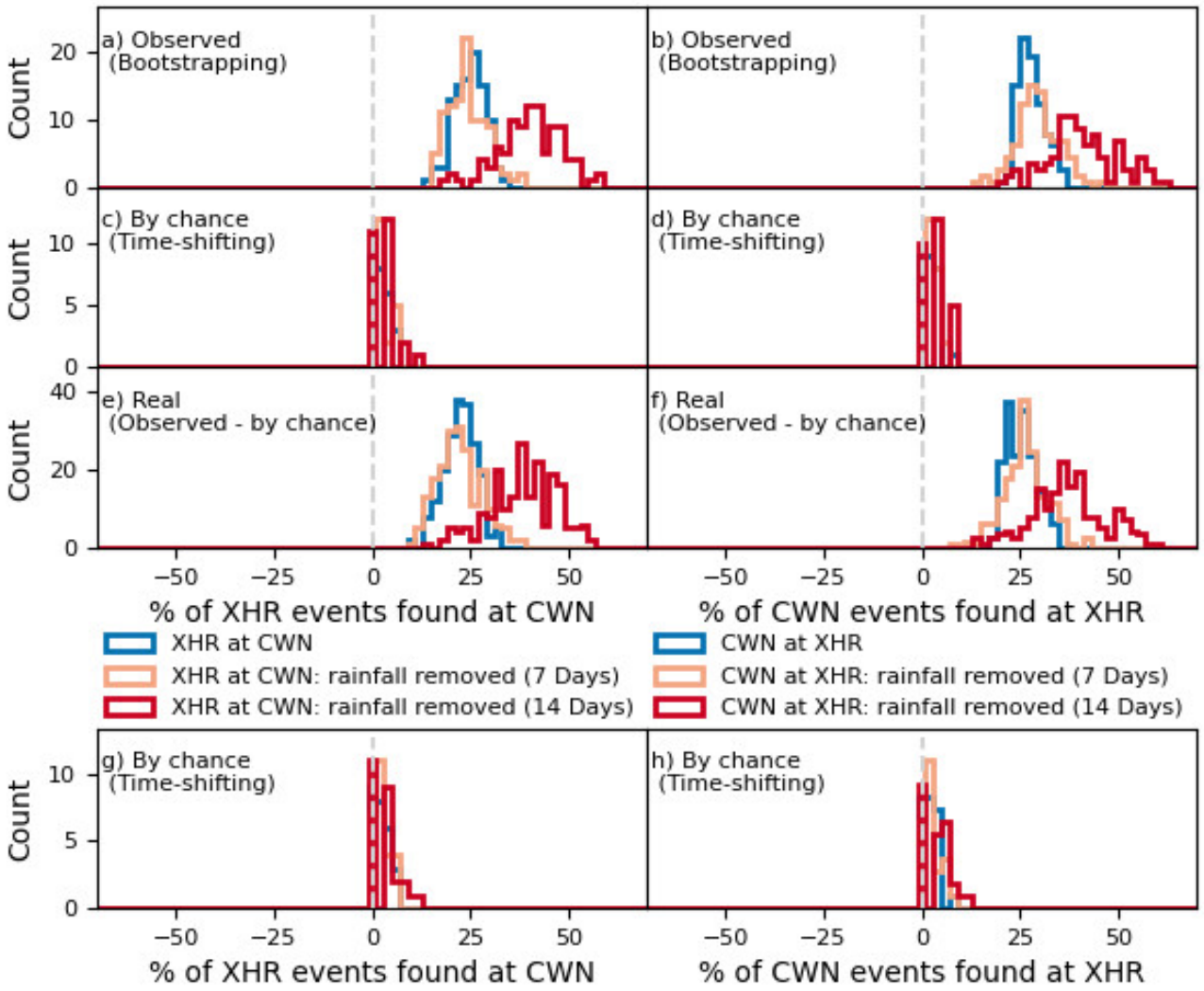

Figure S21. Rainfall analysis histograms for Harris Ranch (XHR) and Cienega Winery (CWN). Blue historgrams are the original analysis before rainfall was removed, orange and red histograms are for when events with rainfall in the 7 or 14 days prior are removed respectively. a) and b) are the bootstrapped distributions of the percentage of events with different amounts of rainfall accounted for. c) and d) shows the percentage of time correlated events that are occuring by chance. e) and f) are percentage of events that are detected at both creepmetes when by chance occurances are removed. g) and h) show the percentage of events that are observed at one creepmeter given seasonality and rain at the other.

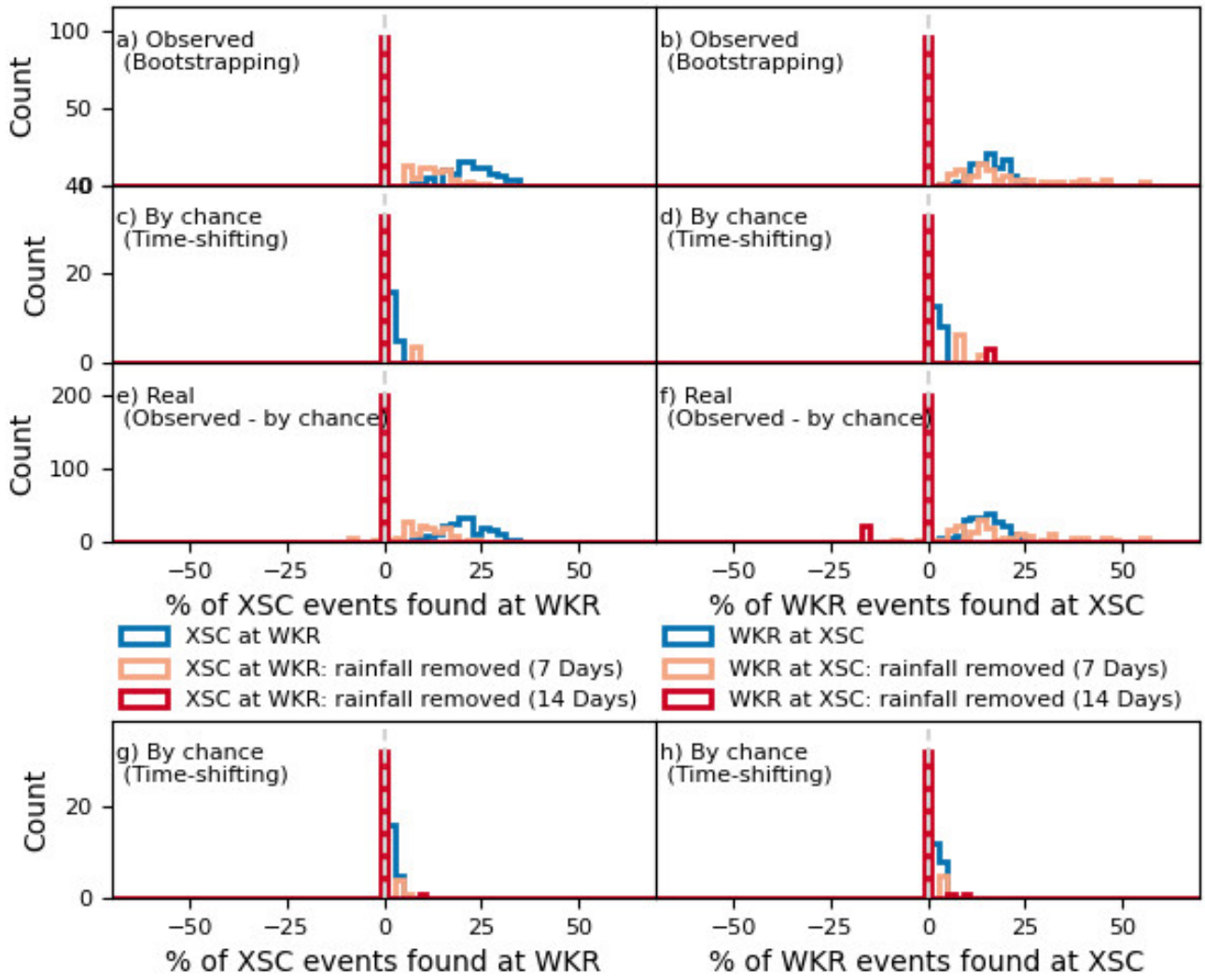

Figure S22. Rainfall analysis histograms for Slacks Canyon (XSC) and Work Ranch (WKR). Blue historgrams are the original analysis before rainfall was removed, orange and red histograms are for when events with rainfall in the 7 or 14 days prior are removed respectively. a) and b) are the bootstrapped distributions of the percentage of events with different amounts of rainfall accounted for. c) and d) shows the percentage of time correlated events that are occuring by chance. e) and f) are percentage of events that are detected at both creepmetes when by chance occurances are removed. g) and h) show the percentage of events that are observed at one creepmeter given seasonality and rain at the other.

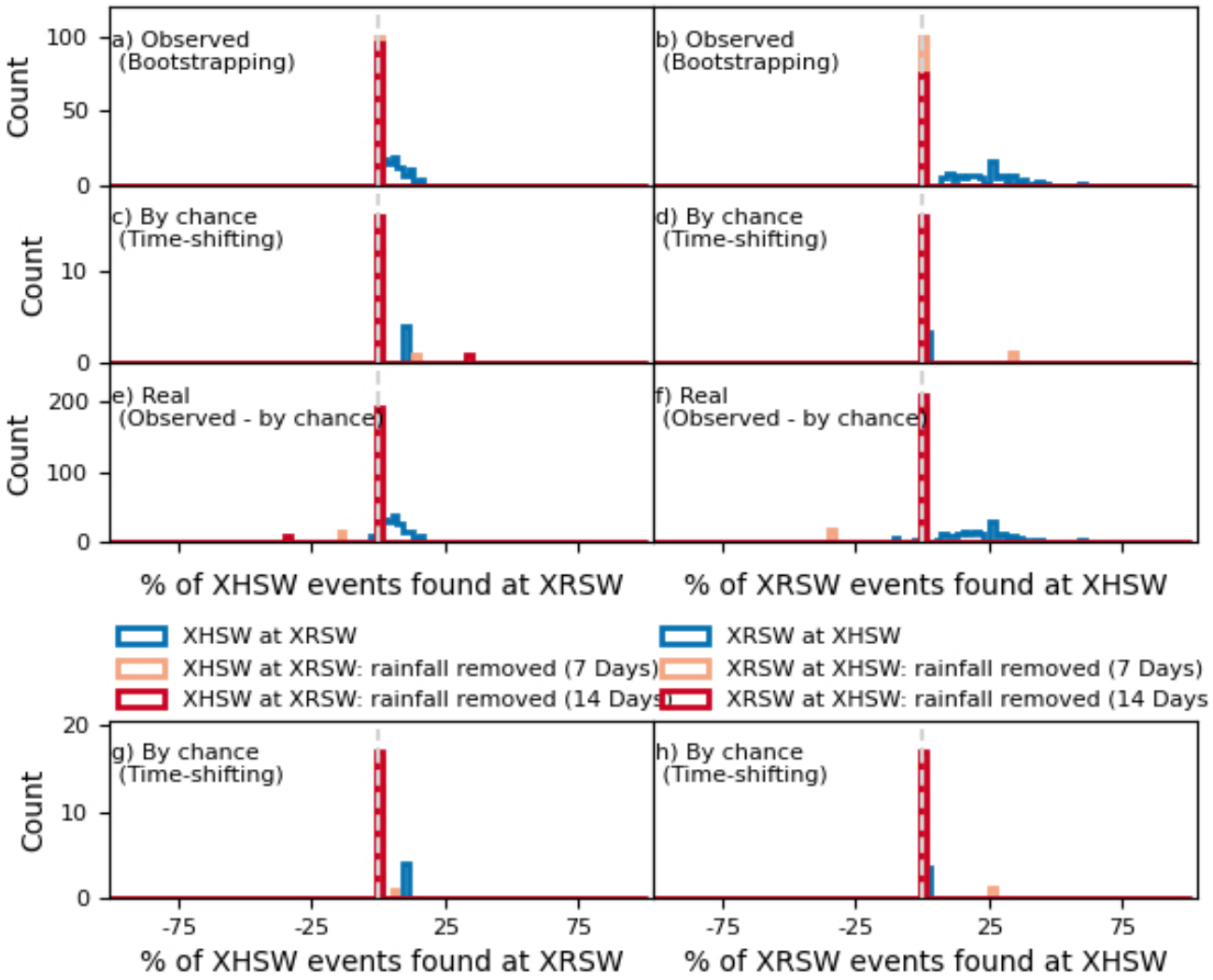

Figure S23. Rainfall analysis histograms for Roberson Southwest (XRSW) and Hearst Southwest (XHSW). Blue historgrams are the original analysis before rainfall was removed, orange and red histograms are for when events with rainfall in the 7 or 14 days prior are removed respectively. a) and b) are the bootstrapped distributions of the percentage of events with different amounts of rainfall accounted for. c) and d) shows the percentage of time correlated events that are occuring by chance. e) and f) are percentage of events that are detected at both creepmetes when by chance occurances are removed. g) and h) show the percentage of events that are observed at one creepmeter given seasonality and rain at the other.

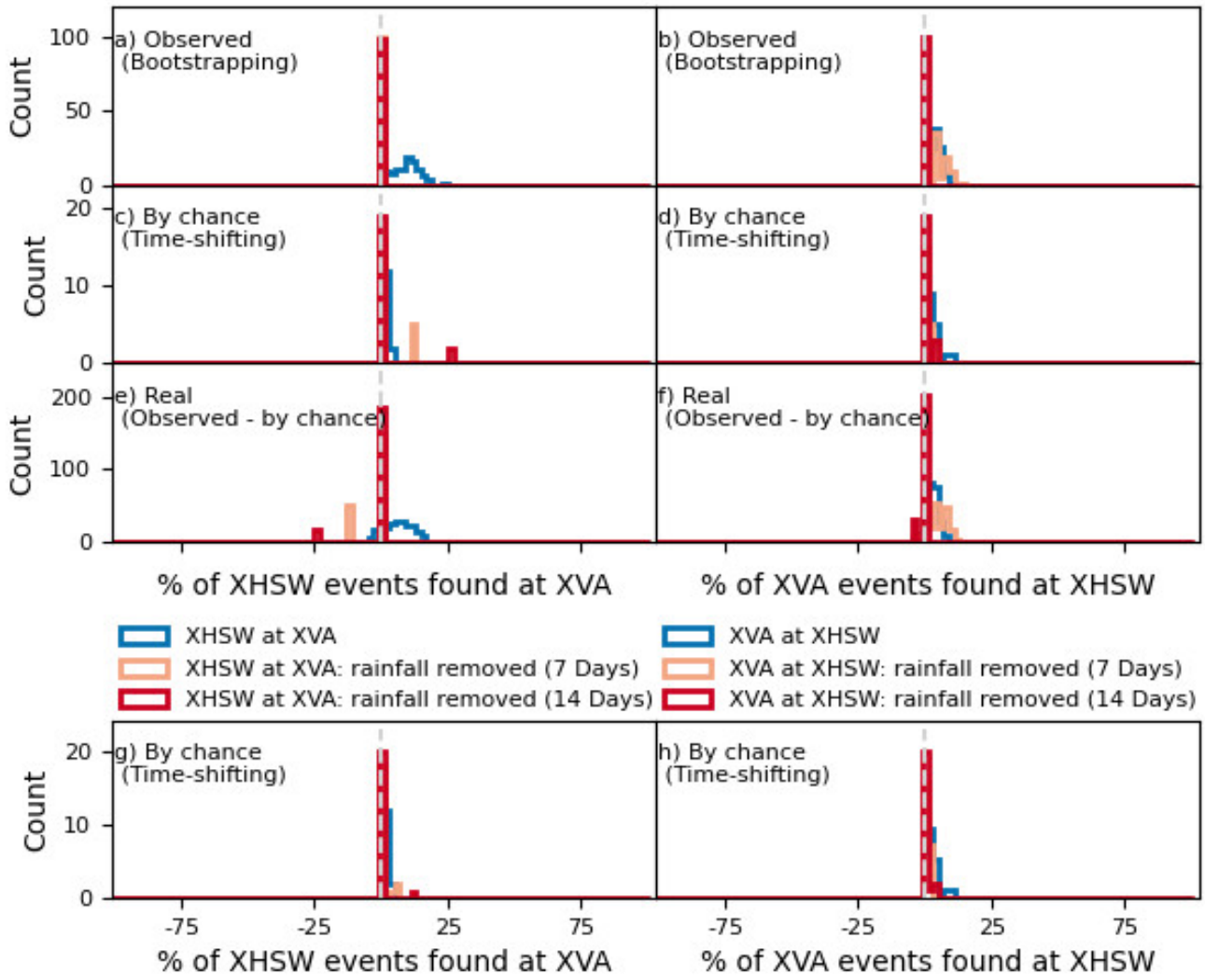

Figure S24. Rainfall analysis histograms for Hearst Southwest (XHSW) and Varian (XVA). Blue historgrams are the original analysis before rainfall was removed, orange and red histograms are for when events with rainfall in the 7 or 14 days prior are removed respectively. a) and b) are the bootstrapped distributions of the percentage of events with different amounts of rainfall accounted for. c) and d) shows the percentage of time correlated events that are occuring by chance. e) and f) are percentage of events that are detected at both creepmetes when by chance occurances are removed. g) and h) show the percentage of events that are observed at one creepmeter given seasonality and rain at the other.

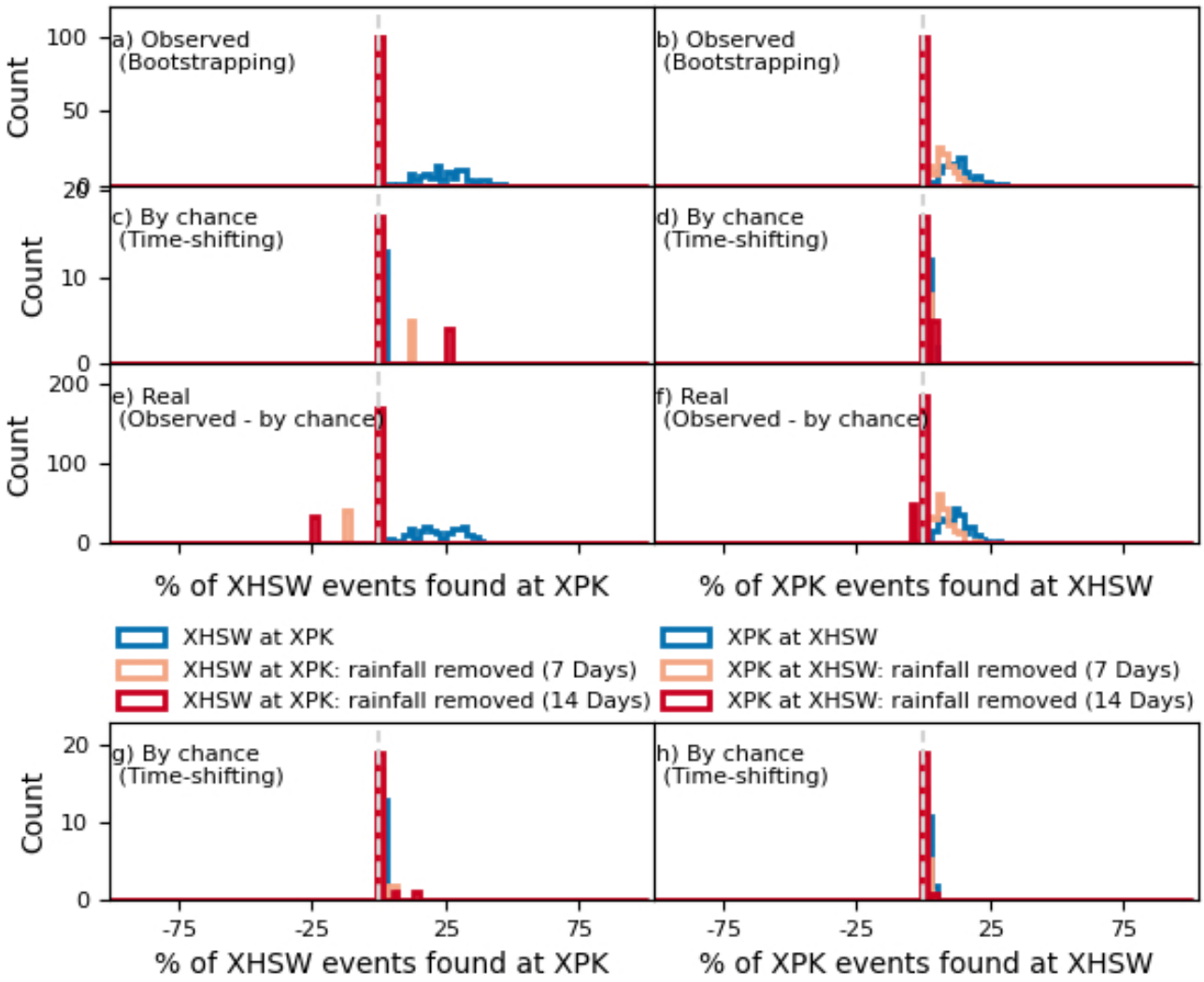

Figure S25. Rainfall analysis histograms for Hearst Southwest (XHSW) and Parkfield (XPK). Blue historgrams are the original analysis before rainfall was removed, orange and red histograms are for when events with rainfall in the 7 or 14 days prior are removed respectively. a) and b) are the bootstrapped distributions of the percentage of events with different amounts of rainfall accounted for. c) and d) shows the percentage of time correlated events that are occuring by chance. e) and f) are percentage of events that are detected at both creepmetes when by chance occurances are removed. g) and h) show the percentage of events that are observed at one creepmeter given seasonality and rain at the other.